ADVANCED FUNCTIONAL MATERIALS
www.afm-journal.de

Compose and Convert: Controlling Shape and Chemical Composition of Self-Organizing Nanocomposites

*Marloes H. Bistervels, Arno van der Weijden, Hinco Schoenmaker, Marko Kamp, and Willem L. Noorduin**

Organizing the right material at the right place has the potential to revolutionize bottom-up assembly of functional architectures. Despite tremendous progress, this is still difficult in particular because control over chemical composition and morphology are typically inherently entangled. Here a two-step strategy is introduced based on self-organization and conversion reactions to shape a wide selection of chemical compositions into user-defined designs. First, photogeneration of CO_2 induces precipitation of nanocomposites of barium carbonate nanocrystals and amorphous silica ($BaCO_3/SiO_2$) with control over shape and location following arbitrary illumination patterns. Second, the resulting nanocrystals are converted by sequential ion exchange into a palette of chemical compositions, while the original shape is preserved. By considering thermodynamic stability and chemical reactivity, orthogonal conversion reactions are designed for sequentially positioning nanocomposites of different metal chalcogenide semiconductors next to each other. Based on these strategies, different compositions are integrated into the same hybrid architecture, and the functionality potential is demonstrated by forming a light-emitting perovskite semiconductor that is embedded into an optical waveguide. Combining light-controlled self-organization and shape-preserving ion-exchange reactions offers exciting opportunities for shaping up materials.

1. Introduction

Organizing the right chemical in the right place is at the core of how organisms steer mundane materials into biominerals with remarkable functionalities.[1–9] While biological processes select building blocks based on evolutionary cues, human-designed self-organization processes can tap into a much wider catalog of materials that include synthetic compositions with semiconducting, optoelectronic, or catalytic properties. Driven by these insights, already many bioinspired processes have been developed to emulate, extend, and exceed the performance of biominerals.[10–19] Nevertheless, despite these successes it remains challenging to achieve independent control over where and in which shape chemical compositions of choice can be sculpted, as the control over shape and chemical composition are traditionally inherently entangled.

We here propose a two-step assembly/conversion strategy to shape desired chemical compositions following predetermined designs (**Figure 1**). In the first step, photodecarboxylation of ketoprofen under UV light (275–365 nm) generates carbonate (CO_2), which steers the acid-regulated coprecipitation of barium carbonate ($BaCO_3$) nanocrystals and amorphous silica (SiO_2) into a nanocomposite according to light-controlled patterns (Figure 1B). In the second step, ion exchange reactions convert the nanocrystals in the nanocomposite while preserving the original morphology and fine features of the original form (Figure 1C). Even more refined and complex control over shaping of different compositions may be possible by developing orthogonal conversion reactions such that consecutive cycles of assembly/conversion can yield complex rationally designed hybrid architectures. In principle, the here proposed strategy should enable independent control over both the shape and chemical composition of user-defined architectures.

Our strategy builds upon previous work on precipitation and conversion reactions of bioinspired $BaCO_3/SiO_2$ nanocomposites.[20–28] These nanocomposites form during the acid-regulated precipitation of $BaCO_3$ nanocrystals and amorphous SiO_2. By modulating the precipitation conditions, a wide diversity of complex shapes can be rationally designed. For instance, nanocomposites with stem-, vase- and coral-like shapes can be formed at a pH of ca. 12, while helices and leave-like shapes can be formed at a pH of ca. 11. These shapes can be further sculpted, patterned and hierarchically organized by modulating the reaction conditions, e.g., CO_2 concentration,

M. H. Bistervels, A. van der Weijden, H. Schoenmaker, M. Kamp, W. L. Noorduin
AMOLF
Science Park 104, Amsterdam 1098 XG, The Netherlands
E-mail: noorduin@amolf.nl
W. L. Noorduin
Van 't Hoff Institute for Molecular Sciences
University of Amsterdam
Science Park 904, Amsterdam 1090 GD, The Netherlands
The ORCID identification number(s) for the author(s) of this article can be found under https://doi.org/10.1002/adfm.202403715

DOI: 10.1002/adfm.202403715

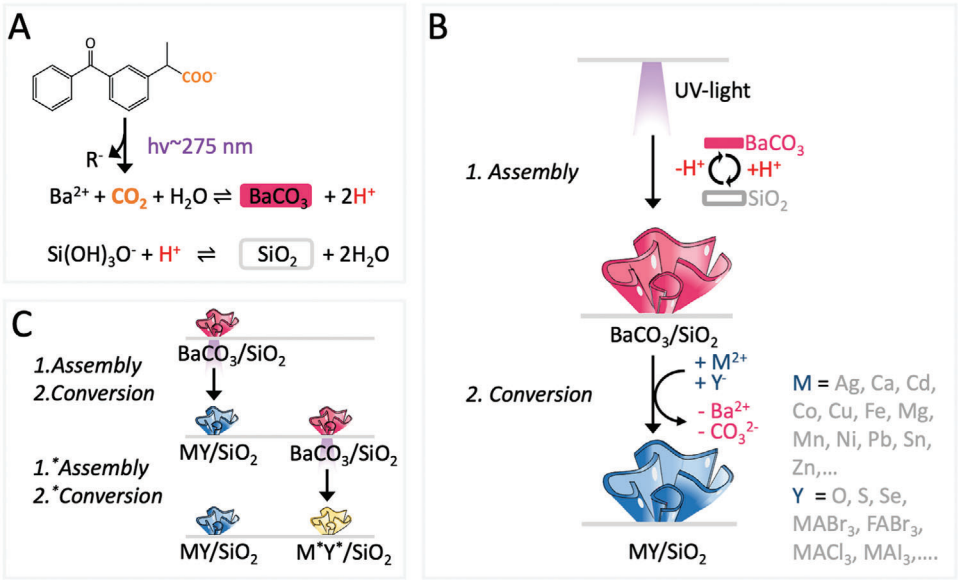

Figure 1. Assembly/conversion strategy for controlling shape and chemical composition of self-organizing nanocomposites. A) UV-irradiation triggers photodecomposition of ketoprofen, resulting in CO_2 generation which in turn onsets the coprecipitation of $BaCO_3$ and SiO_2. B) UV-light steers the assembly of a $BaCO_3/SiO_2$ nanocomposite with light-controlled shapes. Subsequently, the chemical composition of the nanocrystals is converted via a cascade of ion-exchange reactions, which can be chosen from a selection of more than fifty compounds, including metal chalcogenides and perovskites (MA = methyl ammonium, FA = formamidinium). C) Orthogonal assembly/conversion schemes enable positioning and integration of different chemical compositions into user-defined architectures such that for instance the first assembly/conversion into MY/SiO_2 remains unreactive during the sequential assembly/conversion of another $BaCO_3/SiO_2$ shape into M^*Y^*/SiO_2.

temperature, pH during the growth to stack for instance coral forms on helices, or create landscapes with stems that open into vases.[22] Moreover, photogeneration of CO_2 has been developed to control the precipitation process following UV light patterns.[29–31] Once these nanocomposites are formed, we have shown that the chemical composition of $BaCO_3/SiO_2$ nanocomposites can be converted by performing cat- and anion exchange reactions, with preservation of the initial shape and fine details.[32–40] Importantly, these conversion reactions are to a large extent independent of the initial shape of the nanocomposite such that the shape and chemical composition are disentangled and independently controllable. By now, an extensive catalog of conversion pathways has been developed to more than 50 different chemical compositions including many metal chalcogenides, metals, and perovskites.[32–40] The semiconducting, optoelectronic, and catalytic properties of these compositions have been used to achieve a range of functionalities such as catalysts with tunable selectivity.[35–37] However, up to now it has remained unclear if these photochemical precipitation processes and conversion reactions can be combined, let alone if highly selective orthogonal assembly/conversion routes can be developed for consecutive organization of arbitrary chemical compositions in user-defined and functional hybrid architectures.

Motivated by these insights, we here demonstrate that a range of light schemes can be used for precipitating nanocomposites on preassigned locations, shaping complex contours, and drawing arbitrary-shaped lines, all of which subsequently can be converted into a range of metal chalcogenide semiconductors with preservation of microscopic shape and fine details. Moreover, based on the thermodynamic stability and chemical reactivity of different compositions, we design orthogonal conversion pathways to sequentially position nanocomposites of different chemical compositions next to each other. Finally, we show how different compositions can be integrated into the same hybrid architecture and form a light-emitting perovskite semiconductor that is embedded into an optical waveguide to demonstrate the functionality potential of this assembly/conversion strategy.

2. Results and Discussion

We test the compatibility between ion exchange reactions and photoinduced self-organization. To this aim we combine different light schemes for controllable self-assembly with different types of conversion reactions (**Figure 2**). We show three levels of control over semiconductor sculpting by forming an array of coral-shaped cadmium selenide (CdSe), a triangle of cobalt oxide (Co_3O_4), and a line of manganese sulfide (MnS).

We position an array of CdSe coral shapes on preassigned locations by photo-controlled coprecipitation of $BaCO_3/SiO_2$ nanocomposites. To this aim, we create a gradient of carbonate that is too low for nucleation yet sufficiently high for growth. We achieve this by illuminating an area with a radius of 250 µm using low intensity 365 nm UV light with a long penetration depth to photogenerate CO_2. Subsequently, we induce nucleation with a short burst of 275 nm UV light with a short penetration depth that is projected in a 50 µm radius through two lenses from the opposite side inside the area irradiated by 365 nm. Within 15–35 seconds, we observe the formation of a small coral-like form in the area that is illuminated by the 275 nm UV-light (Figure S2A–D, see Supporting Information for details). We repeat this short burst of 275 nm UV light at five other locations to create an array of six coral-shaped nanocomposites on preassigned positions.

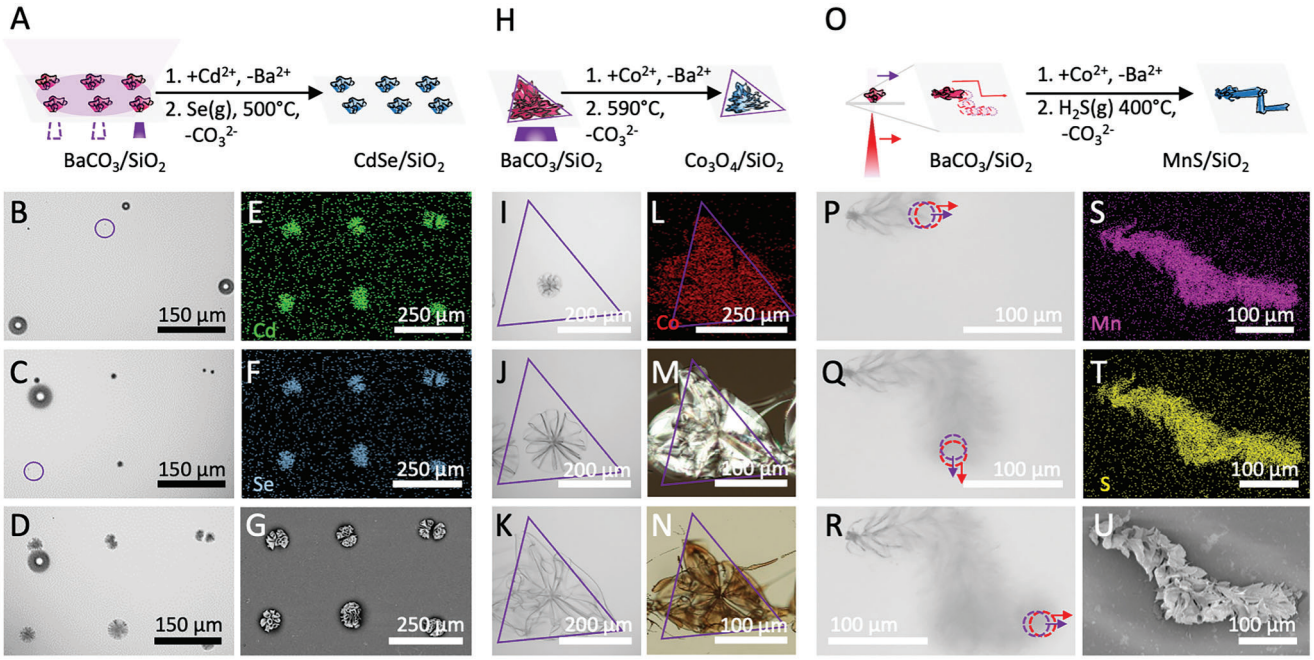

Figure 2. Shape-preserving chemical conversion of light-controlled $BaCO_3/SiO_2$ nanocomposites. A) reaction scheme toward an array of six $CdSe/SiO_2$ coral-shapes. B–D) Optical microscopy time-lapse showing sequential positioning of coral shapes using UV spot (nucleation spot indicated with purple circle). E–G) EDS SEM of cadmium (Cd) and selenium in resulting coral shapes. H) Reaction scheme toward a Co_3O_4/SiO_2 triangle. I–K) Optical microscopy time-lapse showing the formation of a triangle-shaped nanocomposite within the triangle shaped UV-pattern (indicated in purple). L) EDS SEM map showing cobalt (Co). M) Optical polarization microscopy of the original $BaCO_3/SiO_2$ form. N) Optical microscopy of the converted Co_3O_4/SiO_2 form that is shrunken. O) Reaction scheme for MnS/SiO_2 line. P–R) Optical microscopy time-lapse showing precipitation following a moving UV and IR spot (depicted in purple and red respectively). S–U) EDS SEM analysis showing manganese (Mn) and sulfide (S) in the resulting line-shape.

Note that for each nanocomposite we adjust the light-intensity, as during the experiment precursor depletion, photoproduct accumulation, and silica oligomerization change the conditions such that longer and stronger UV-light irradiation is needed to locally generate sufficient CO_2 for nucleation and growth.

We convert this array of coral shapes from $BaCO_3$ into CdSe. Following previously developed methods,[38] we first perform cation exchange of barium to cadmium by immersing the array in a solution containing cadmium ions (50 mM). Subsequently, we perform anion exchange of carbonate to selenium (Se^{2-}) by exposing the array to selenium gas. Energy Dispersion Spectroscopy (EDS) is consistent with complete conversion of $BaCO_3$ to CdSe, while Scanning Electron Microscopy (SEM) shows excellent preservation of the 3D shape and fine features (Figure 2E–G).

To form a triangular-shaped architecture composed of Co_3O_4, we project a triangle light pattern of 275 nm (75 µW mm^{-2}) and induce nucleation and growth (Figure S2H–K, see Supporting Information for details). After 5.5 h we observe a $BaCO_3/SiO_2$ architecture with the contours of the geometric light pattern. The $BaCO_3$ nanocrystals are converted into Co_3O_4 in two steps. First, we exchange barium for cobalt to yield the triangle shape made of basic cobalt carbonate (see Supporting Information for details). Second, we form the desired Co_3O_4 by heating the nanocomposite in air at 540 °C (Figure S2H,L, see Supporting Information for details). During the conversion the crystal lattice volume would theoretically shrink with ca. 17%.[40] We find indeed that the structure visibly shrinks, but that it remains completely intact with all fine features preserved (Figure 2M,N).

We explore the versatility of light schemes that can be used in combination with ion-exchange. From this perspective, it is particularly interesting to combine UV-induced local photogeneration of CO_2 with near-infrared (NIR) induced local heating. Since for increasing temperatures the precipitation rates of $BaCO_3$ and SiO_2 increase, this local heating can speed up the precipitation and thereby refine the resolution, while the smaller feature sizes may enable steering the precipitate in curves.[29] However, local heating can also enhance cross-linking of the SiO_2 matrix, which in turn may potentially hinder subsequent ion-exchange reactions.[36]

To investigate this scenario, we form a manganese sulfide (MnS) line-shape nanocomposite. We induce precipitation by combining a 365 nm UV LED via the objective and a 1435 nm NIR laser diode via two lenses from the opposite site to locally generate CO_2 and heat the solution respectively. By modulating the light intensity (Figure S2O–R, see Supporting Information for details), we draw an arbitrarily shaped line. To demonstrate the achievable fidelity, we make two 90 ° turns. Subsequently we convert the line into MnS, following previously developed conversion reactions.[36] Even though the local heating may induce further crosslinking of the SiO_2 matrix, we find that the $BaCO_3$ nanocrystals straightforwardly undergo ion exchange to manganese carbonate ($MnCO_3$), which subsequently convert to MnS upon exposure to hydrogen disulfide gas (H_2S). EDS and SEM of the resulting structure shows that the curvatures of the corners have changed—likely due to the mechanical forces that are exerted during the shrinking of the crystal lattice volume during

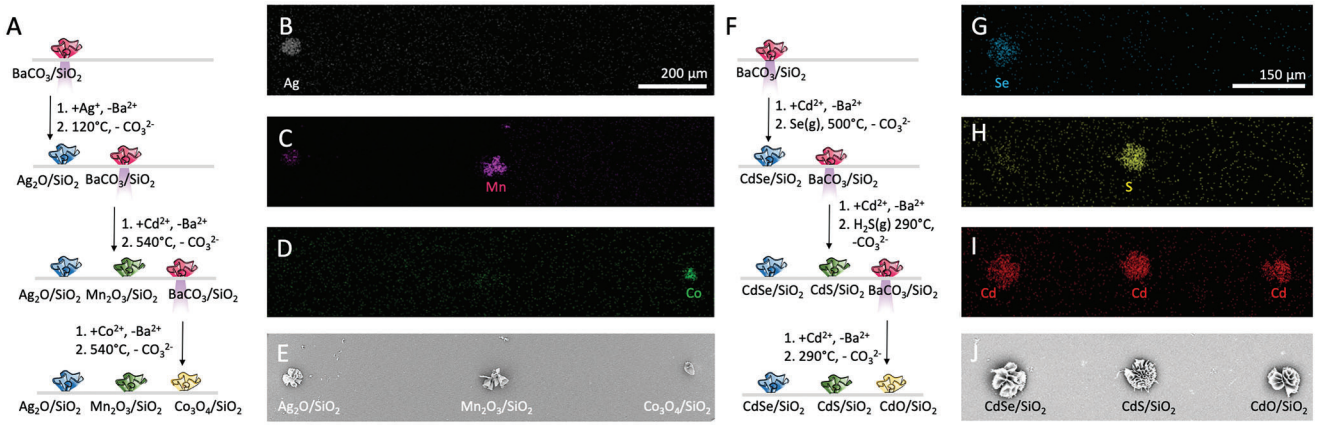

Figure 3. Orthogonal conversion reactions for positioning multiple chemical compositions. A) Reaction scheme for orthogonal cation exchange toward an array of Ag_2O/SiO_2, Mn_2O_3/SiO_2, and Co_3O_4/SiO_2 coral shapes. B–E) EDS-SEM analysis of the resulting structures showing selective cation exchange to (B) silver (Ag); C) manganese (Mn); and D) cobalt (Co). F) Reaction scheme for orthogonal anion exchange toward an array of $CdSe/SiO_2$, CdS/SiO_2, and CdO/SiO_2 coral shapes. G–J) EDS-SEM analysis of the resulting structures showing selective anion exchange to G) selenium (Se); H); sulfide S); and I) cation exchange to cadmium (Cd). Note that oxygen does not show up on EDS.

the conversion. Nevertheless, we still find complete conversion (Figure S2S-U, see Supporting Information for details), showing that the conversion reactions and different light-schemes are compatible.

This compatibility opens the opportunity for sequential series of photo-induced self-organization and conversion reactions such that for instance, an array of different chemical compositions can be positioned on predetermined locations next to each other. However, such sequential series can only be performed using orthogonal reaction pathways to avoid that earlier formed structures undergo ion exchange. To develop such orthogonal reaction pathways, we realize that in water the solubilities of metal carbonates are orders of magnitude larger than those of metal chalcogenides. Consequently, metal carbonates may be prone to undergo ion exchange under conditions in which metal chalcogenides remain unreactive, which may facilitate sequential orthogonal cation-exchange pathways.

To test the concept of such orthogonal cation-exchange pathways, we position coral-shapes of three different semiconductor compositions next to each other (**Figure 3**). To form the first coral shape, we photochemically induce the precipitation of a coral-like shape. We convert the $BaCO_3$ into silver carbonate (Ag_2CO_3), which subsequently reacts to silver oxide (Ag_2O) under heating at 120 °C in a nitrogen atmosphere (Figure S3A,B, see Supporting Information for details). Following a similar photochemical scheme, we position a second coral shape next to the first one. Importantly, the precision of the photochemistry allows us to avoid precipitation on the earlier formed Ag_2O coral, while the low reactivity of Ag_2O prevents undesired ion-exchange with the carbonate and barium ions in the solution. After growing the second coral-shape, we convert it to $MnCO_3$, followed by thermal decomposition to Mn_2O_3 at 540 °C in an aerobic atmosphere, thereby simultaneously reducing the silver oxide coral shape to metallic silver (Figure 3A,C). Finally, a third coral shape is precipitated, equidistantly spaced next to the Ag and Mn_2O_3 corals. This coral is converted via basic cobalt carbonate into Co_3O_4, while leaving the earlier formed corals intact (Figure 3A,D). EDS analysis confirms that only trace amounts of cross exchange has occurred, hence demonstrating that orthogonal sequences of photoinduced precipitation and cation-exchange reactions are possible (Figure 3B-E).

While orthogonal cation exchange pathways can be designed based on thermodynamic stability, we find that orthogonal anion conversion pathways can be rationally planned following chemical reactivity. Specifically, we realize that many metal carbonates react toward metal sulfides at temperatures and partial H_2S pressures for which metal selenides remain unreactive for anion exchange. Moreover, many metal carbonates react to metal oxides at temperatures at which metal sulfides and selenides remain unreactive. This suggests that orthogonal pathways for different anion reactions may be feasible.

We exploit this insight by designing a pathway of orthogonal anion reactions to position coral shapes of cadmium selenide (CdSe), cadmium sulfide (CdS) and cadmium oxide (CdO) (Figure 3F). We position a first coral shape and convert this coral to CdSe (Figure 3F,G). We position a second coral shape next to the first one, and convert this shape to $CdCO_3$. Subsequently these shapes are exposed to H_2S gas at 290 °C. Under these reaction conditions, the CdSe remains unreactive, while EDS shows complete conversion of the $CdCO_3$ to CdS (Figure 3F,H). Finally, we position a third coral shape at equidistant spacing of the already formed CdS and CdSe coral shape. Again, the $BaCO_3$ in the coral is converted into $CdCO_3$ and then heated to 290 °C, which results in the conversion to CdO while leaving the CdS and CdSe structures unreacted. Hence, orthogonal anion reaction pathways can be designed by judiciously selecting sequences of reaction conditions.

The combination of spatiotemporal control over self-organization and orthogonal shape-preserving conversion reactions presents the opportunity for the creation of hybrid materials in which different nanocrystals of preselected chemical compositions are integrated within a single nanocomposite (**Figure 4**). We exploit these insights to form an integrated hybrid structure composed of a CdSe triangle and Ag circle (Figure 4A-D). Using a photomask, we first induce growth of a triangular nanocomposite, which we convert to CdSe (see

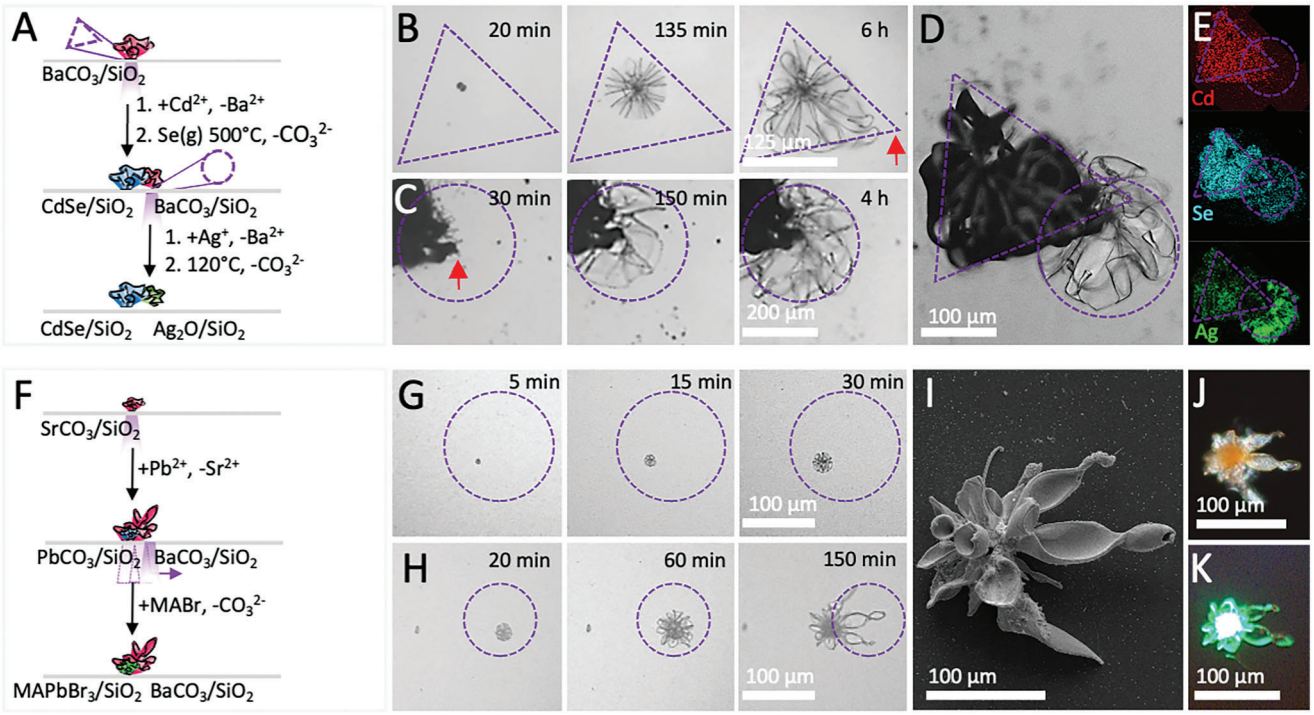

Figure 4. Integration of different compositions within a single nanocomposite. A) Reaction scheme for integration of Ag_2O/SiO_2 circle and $CdSe/SiO_2$ triangle shape via light-controlled assembly and orthogonal conversion reactions. B) Optical microscopy time-lapse showing the assembly of the triangle shape. C) Optical microscopy time-lapse showing the assembly of the circle shape after conversion of the triangle into $CdSe/SiO_2$. The red arrow in B and C indicates the same location. D) Optical microscopy image after conversion of the Ag_2O/SiO_2 circle and $CdSe/SiO_2$ triangle. E) EDS-SEM map showing confirming Cd and Se in the triangle and Ag in the circle. F) Reaction scheme for integration of $MAPbBr_3/SiO_2$ coral into an elongated $BaCO_3/SiO_2$ shape. G) Optical microscopy time-lapse showing the assembly of the $SrCO_3/SiO_2$ coral. (H) Optical microscopy time-lapse showing the assembly of the elongated $BaCO_3/SiO_2$ structure by moving the UV spot away from the initial coral shape that is converted into $PbCO_3/SiO_2$. I) SEM of the final hybrid $BaCO_3/SiO_2$ composite with integrated light emitting $MAPbBr_3/SiO_2$ core. J) Polarized microscopy image showing that the nanocrystals are not aligned, and K) fluorescence microscopy showing photoluminescence from hybrid $BaCO_3/SiO_2$ with light emitting $MAPbBr_3/SiO_2$ core.

Supporting Information). We then project a circular UV-light pattern with a radius of 100 µm on the corner of the triangular-shaped CdSe and induce nucleation. We observe new nucleation exclusively on top of the edges of the already grown and converted CdSe triangle, likely because exposed nanocrystals favor nucleation at these locations. We continue growth until the contours of the circle are filled. We subsequently convert the $BaCO_3$ in the circle to $AgCO_3$. Consistent with our orthogonal conversion scheme, the low solubility product of CdSe prevents conversion of the triangle. Subsequent heating to 120° C results in the conversion of the circle to Ag_2O while the triangle remains CdSe, thus forming a shape-controlled hybrid structure (Figure 4E).

The combination of spatiotemporal control and orthogonal chemistry can be used to integrate synergistic properties within a single architecture with independent control over shape and composition of the separate parts. Building upon our previous work with optical structures,[24] we demonstrate this potential by integrating a light-emitting lead methyl ammonium bromide perovskite ($MAPbBr_3$) semiconductor with a $BaCO_3/SiO_2$ shape that serves as optical waveguide (Figure 4F-K). To form the light-source, we induce the nucleation and growth of a small coral-shaped nanocomposite. Instead of $BaCO_3$, we precipitate strontium carbonate ($SrCO_3$). $SrCO_3$ has similar properties as $BaCO_3$, but the smaller crystal lattice facilitates straightforward ion-exchange to perovskite precursor $PbCO_3$. We subsequently focus a 365 nm UV light top of the $PbCO_3/SiO_2$ structure and induce precipitation of $BaCO_3/SiO_2$. After 60 min, we move the UV spot to selectively direct the growth to one side into an elongated shape with a tip. Finally, we immerse the resulting structure into methyl ammonium bromide to convert the $PbCO_3$ into a methylammonium bromide perovskite semiconductor. SEM, EDS, and light microscopy using crossed polarizers confirm that lead is only present in the bottom part while the nanoscopic crystallographic alignment is lost, but the microscopic shape remains preserved (Figure S4I-J, see Supporting Information for details). The final architecture performs waveguiding of the light emitted from the perovskite core toward the tip of the elongated shape (Figure 4K).

3. Conclusion

We here demonstrate how light-driven self-organization processes and ion-exchange reactions can be combined to gain independent control over shape and composition. This two-step assembly/conversion strategy allows us to position, sculpt and hierarchically organize a wide range of metal oxides, metal sulfides, and perovskites according to light-controlled designs. Complex

hybrid architectures and landscapes of preassigned palettes can be formed by consecutively assembling and converting nanocomposites using orthogonal reaction pathways with independent control over shape and composition of each component.

Our assembly/conversion strategy takes advantage of fundamental features of self-organization. In traditional synthesis processes shape and composition are inherently entangled such that for each composition a new method is required to control the shape. In contrast, in our assembly/conversion strategy the self-organization process autonomously generates and orders nanoscopic building blocks. Because of this inherent nanostructure, these architectures subsequently can be converted into a wide catalog of chemical compositions independent of their initial shape. The self-organized nanostructure is essential for these shape-preserving conversions: the nanocrystals offer enhanced chemical reactivity while the nanocomposite layout fascilitates transport of reactants and offers mechanical stability for complete conversion with preservation of the initial shape.

By decoupling the control of shape and composition, our multistep self-organization strategy gives spatiotemporal control over where which chemical composition is positioned. Photochemical reactions provide hands-on control over positioning and shaping, while orthogonal conversion pathways enable integration of different chemical compositions independent of their shape in sequential steps for the synthesis of complex hybrid components. This work adds to an expanding collection of self-organization strategies that have been coined non-covalent synthesis.[41,42] Akin to organic chemistry—in which covalent bonds are rationally designed at molecular scale using for instance protection groups, reactive centra and reaction cascades, we here are learning how non-covalent interactions can be precisely controlled at nano- and microscale via multistep reaction pathways to shape, convert, orient and construct increasingly complex components and devices.

Indeed, we foresee that further control over the assembly/conversion process is possible. In particular, for the assembly step two-photon or light-sheet illumination schemes may offer refined control over the self-organization in three spatial dimensions. Moreover, for the conversion step, the continuously growing catalog of conversion pathways[35–40,43,44]—which currently provide routes to more than fifty different chemical compositions including perovskites, metal chalcogenides and metals, that have desirable catalytic, photochemical or electronic functionalities—can be further expanded and refined.

Beyond these coprecipitation reactions, we anticipate that other self-organizing systems such as Liesegang inspired patterns and chemical gardens can be controlled using this assembly/conversion strategy.[43–48] Specifically, we believe that light-induced chemical conversion can be developed, akin to classical photography techniques, to pattern different chemical compositions into preformed substrates. Also, assembly/conversion strategies can leverage the complexity and seemingly effortless control by biomineralizing organisms. These conversion routes can already be used to convert biomineralized skeletons.[35,38,49,50] We foresee that biomineralization processes can be influenced and steered using light patterns using for instance IR.[30] These opportunities are highlighting new pathways for advanced and functional components, with refined hands-on control when needed, and effortless self-organization when possible.

Supporting Information

Supporting Information is available from the Wiley Online Library or from the author.

Acknowledgements

M.H.B. and A.v.d.W. contributed equally to this work. This work is part of the Vernieuwingsimpuls Vidi research program "Shaping up materials" with project number 016.Vidi.189.083, which is partly financed by the Dutch Research Council (NWO).

Conflict of Interest

The authors declare no conflict of interest.

Data Availability Statement

The data that support the findings of this study are available in the supplementary material of this article.

Keywords

bio-inspired mineralization, light-induced crystallization, ion-exchange reactions, nanocomposites, self-organisation

Received: February 29, 2024
Revised: March 25, 2024
Published online:

[1] H. A. Lowenstam, S. Weiner, *On Biomineralization*, Oxford University Press, New York, USA **1989**.
[2] T. Yang, H. Chen, Z. Jia, Z. Deng, L. Chen, E. M. Peterman, J. C. Weaver, L. Li, *Science.* **2022**, *375*, 647.
[3] Y. F. Xu, F. Nudelman, E. D. Eren, M. J. M. Wirix, B. Cantaert, W. H. Nijhuis, D. Hermida-Merino, G. Portale, P. H. H. Bomans, C. Ottmann, H. Friedrich, W. Bras, A. Akiva, J. P. R. O. Orgel, F. C. Meldrum, N. Sommerdijk, *Nat. Commun.* **2020**, *11*, 5068.
[4] P. U. P. A. Gilbert, K. D. Bergmann, N. Boekelheide, S. Tambutté, T. Mass, F. Marin, J. F. Adkins, J. Erez, B. Gilbert, V. Knutson, M. Cantine, J. O. Hernández, A. H. Knoll, *Sci. Adv.* **2022**, *8*, eabl9653.
[5] E. Beniash, C. A. Stifler, C.-Y. Sun, G. S. Jung, Z. Qin, M. J. Buehler, P. U. P. A. Gilbert, *Nat. Commun.* **2019**, *10*, 4383.
[6] M. Connors, T. Yang, A. Hosny, Z. Deng, F. Yazdandoost, H. Massaadi, D. Eernisse, R. Mirzaeifar, M. N. Dean, J. C. Weaver, C. Ortiz, L. Li, *Nat. Commun.* **2019**, *10*, 5413.
[7] Y. Cui, H. Li, Y. Li, L. Mao, *Nanoscale Adv.* **2022**, *4*, 334.
[8] M. Albéric, E. Zolotoyabko, O. Spaeker, C. Li, M. Tadayon, C. N. Z. Schmitt, Y. Politi, L. Bertinetti, P. Fratzl, *Cryst. Growth Des.* **2022**, *22*, 3727.
[9] L. Addadi, S. Weiner, *Phys. Scr.* **2014**, *89*, 098003.
[10] U. G. K. Wegst, H. Bai, E. Saiz, A. P. Tomsia, R. O. Ritchie, *Nat. Mater.* **2015**, *14*, 23.
[11] A. Arakaki, K. Shimizu, M. Oda, T. Sakamoto, T. Nishimura, T. Kato, *Org. Biomol. Chem.* **2015**, *13*, 974.
[12] J. Aizenberg, P. Fratzl, *Adv. Mater.* **2009**, *21*, 387.
[13] X. Wu, F. C. Meldrum, K. Skipper, Y. Yang, C. P. Royall, **2023**. https://arxiv.org/abs/2303.09029u

[14] F. Nudelman, N. A. J. M. Sommerdijk, *Angew. Chemie. – Int. Ed.* **2012**, *51*, 6582.
[15] W. Huang, D. Restrepo, J. Jung, F. Y. Su, Z. Liu, R. O. Ritchie, J. McKittrick, P. Zavattieri, D. Kisailus, *Adv. Mater.* **2019**, *31*, 1901561.
[16] Z. Liu, M. A. Meyers, Z. Zhang, R. O. Ritchie, *Prog. Mater. Sci.* **2017**, *88*, 467.
[17] A. Rao, H. Cölfen, *Morphology Control and Molecular Templates in Biomineralization*, Elsevier, Amsterdam, Netherlands **2016**.
[18] D. Nepal, S. Kang, K. M. Adstedt, K. Kanhaiya, M. R. Bockstaller, L. C. Brinson, M. J. Buehler, P. V. Coveney, K. Dayal, J. A. El-Awady, L. C. Henderson, D. L. Kaplan, S. Keten, N. A. Kotov, G. C. Schatz, S. Vignolini, F. Vollrath, Y. Wang, B. I. Yakobson, V. V. Tsukruk, H. Heinz, *Nat. Mater.* **2023**, *22*, 18.
[19] S. Elsharkawy, A. Mata, *Adv. Healthcare Mater.* **2018**, *7*, 1800178.
[20] J. M. García-Ruiz, E. Melero-García, S. T. Hyde, *Science.* **2009**, *323*, 362.
[21] M. Kellermeier, H. Cölfen, J. M. García-Ruiz, *Eur. J. Inorg. Chem.* **2012**, *2012*, 5123.
[22] W. L. Noorduin, A. Grinthal, L. Mahadevan, J. Aizenberg, *Science.* **2013**, *340*, 832.
[23] J. Opel, M. Hecht, K. Rurack, J. Eiblmeier, W. Kunz, H. Cölfen, M. Kellermeier, *Nanoscale.* **2015**, *7*, 17434.
[24] C. N. Kaplan, W. L. Noorduin, L. Li, R. Sadza, L. Folkertsma, J. Aizenberg, L. Mahadevan, *Science.* **2017**, *355*, 1395.
[25] P. Knoll, O. Steinbock, *Isr. J. Chem.* **2018**, *58*, 682.
[26] M. Montalti, G. Zhang, D. Genovese, J. Morales, M. Kellermeier, J. M. Garciá-Ruiz, *Nat. Commun.* **2017**, *8*, 14427.
[27] T. Terada, S. Yamabi, H. Imai, *J. Cryst. Growth.* **2003**, *253*, 435.
[28] E. Bittarello, D. Aquilano, *Eur. J. Mineral.* **2007**, *19*, 345.
[29] M. H. Bistervels, M. Kamp, H. Schoenmaker, A. M. Brouwer, W. L. Noorduin, *Adv. Mater.* **2022**, *34*, 2107843.
[30] M. H. Bistervels, B. Antalicz, M. Kamp, H. Schoenmaker, W. L. Noorduin, *Nat. Commun.* **2023**, *14*, 6350.
[31] M. H. Bistervels, N. T. Hoogendoorn, M. Kamp, H. Schoenmaker, A. M. Brouwer, W. L. Noorduin, *Nanoscale.* **2024**, *16*, 2310.
[32] J. Opel, L. C. Rosenbaum, J. Brunner, A. Staiger, R. Zimmermanns, M. Kellermeier, T. Gaich, H. Cölfen, J. M. García-Ruiz, *J. Mater. Chem. B.* **2020**, *8*, 4831.
[33] J. Opel, F. P. Wimmer, M. Kellermeier, H. Cölfen, *Nanoscale Horiz.* **2016**, *1*, 144.
[34] J. Opel, J. Brunner, R. Zimmermanns, T. Steegmans, E. Sturm, M. Kellermeier, H. Cölfen, J. M. García-Ruiz, *Adv. Funct. Mater.* **2019**, *29*, 1902047.
[35] T. Holtus, L. Helmbrecht, H. C. Hendrikse, I. Baglai, S. Meuret, G. W. P. Adhyaksa, E. C. Garnett, W. L. Noorduin, *Nat. Chem.* **2018**, *10*, 740.
[36] H. C. Hendrikse, A. van der Weijden, M. Ronda-Lloret, T. Yang, R. Bliem, N. R. Shiju, M. van Hecke, L. Li, W. L. Noorduin, R. Bliem, M. van Hecke, *Adv. Mater.* **2020**, *32*, 2003999.
[37] H. C. Hendrikse, A. Aguirre, A. Van Der Weijden, A. S. Meeussen, F. Neira D'Angelo, W. L. Noorduin, *Cryst. Growth Des.* **2021**, *21*, 4299.
[38] A. van der Weijden, A. S. Léonard, W. L. Noorduin, *Chem. Mater.* **2023**, *35*, 2394.
[39] H. C. Hendrikse, S. Hémon-Charles, L. Helmbrecht, E. P. Van Dam, E. C. Garnett, W. L. Noorduin, *Cryst. Growth Des.* **2021**, *21*, 4500.
[40] A. Van Der Weijden, M. Van Hecke, W. L. Noorduin, *Cryst. Growth Des.* **2022**, *22*, 2289.
[41] G. M. Whitesides, E. E. Simanek, J. P. Mathias, C. T. Seto, D. N. Chin, M. Mammen, D. M. Gordon, *Acc. Chem. Res.* **1995**, *28*, 37.
[42] G. Vantomme, E. W. Meijer, *Science.* **2019**, *363*, 1396.
[43] B. C. Batista, O. Steinbock, *Chem. Commun.* **2022**, *58*, 12736.
[44] Q. Wang, O. Steinbock, *Phys. Chem. Chem. Phys.* **2022**, *24*, 14538.
[45] C. T. van Campenhout, H. Schoenmaker, M. van Hecke, W. L. Noorduin, *Adv. Mater.* **2023**, *35*, 2305191.
[46] B. C. Batista, A. Z. Morris, O. Steinbock, *Proc. Natl. Acad. Sci. USA.* **2023**, *120*, 2017.
[47] B. Aslanbay Guler, Z. Demirel, E. Imamoglu, *Langmuir.* **2023**, *39*, 13611.
[48] L. M. Barge, S. S. S. Cardoso, J. H. E. Cartwright, G. J. T. Cooper, L. Cronin, A. De Wit, I. J. Doloboff, B. Escribano, R. E. Goldstein, F. Haudin, D. E. H. Jones, A. L. Mackay, J. Maselko, J. J. Pagano, J. Pantaleone, M. J. Russell, C. I. Sainz-Díaz, O. Steinbock, D. A. Stone, Y. Tanimoto, N. L. Thomas, *Chem. Rev.* **2015**, *115*, 8652.
[49] D. Palin, R. W. Style, J. Zlopaša, J. J. Petrozzini, M. A. Pfeifer, H. M. Jonkers, E. R. Dufresne, L. A. Estroff, *J. Am. Chem. Soc.* **2021**, *143*, 3439.
[50] A. S. Schenk, I. Zlotnikov, B. Pokroy, N. Gierlinger, A. Masic, P. Zaslansky, A. N. Fitch, O. Paris, T. H. Metzger, H. Cölfen, P. Fratzl, B. Aichmayer, *Adv. Funct. Mater.* **2012**, *22*, 4668.